ACS APPLIED MATERIALS & INTERFACES

Research Article

Cite This: ACS Appl. Mater. Interfaces 2017, 9, 38687-38694

www.acsami.org

Liquid–Solid Dual-Gate Organic Transistors with Tunable Threshold Voltage for Cell Sensing

Yu Zhang,[†] Jun Li,[‡] Rui Li,[§] Dan-Tiberiu Sbircea,[‡] Alexander Giovannitti,[‡] Junling Xu,[†] Huihua Xu,[†] Guodong Zhou,[†] Liming Bian,[§] Iain McCulloch,[∥] and Ni Zhao*[,†]

[†]Department of Electronic Engineering and [§]Department of Biomedical Engineering, The Chinese University of Hong Kong, Shatin, New Territories, Hong Kong

[‡]Department of Chemistry and Centre for Plastic Electronics, Imperial College, London SW7 2AZ, U.K.

[∥]King Abdullah University of Science and Technology (KAUST), KSC, Thuwal 23955-6900, Saudi Arabia

Supporting Information

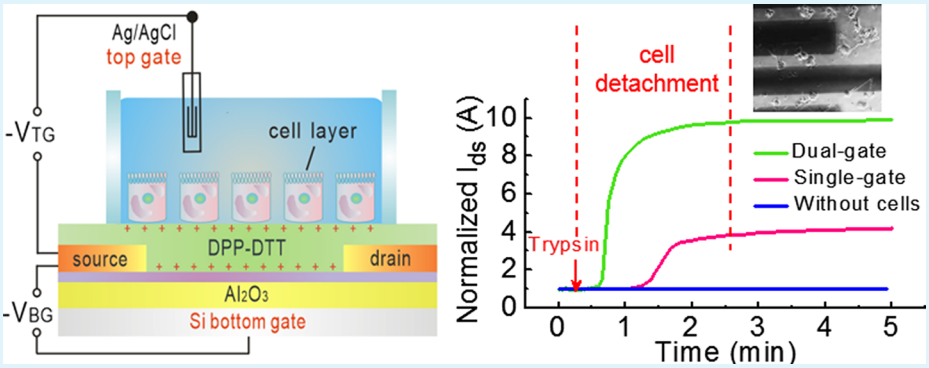

ABSTRACT: Liquid electrolyte-gated organic field effect transistors and organic electrochemical transistors have recently emerged as powerful technology platforms for sensing and simulation of living cells and organisms. For such applications, the transistors are operated at a gate voltage around or below 0.3 V because prolonged application of a higher voltage bias can lead to membrane rupturing and cell death. This constraint often prevents the operation of the transistors at their maximum transconductance or most sensitive regime. Here, we exploit a solid–liquid dual-gate organic transistor structure, where the threshold voltage of the liquid-gated conduction channel is controlled by an additional gate that is separated from the channel by a metal-oxide gate dielectric. With this design, the threshold voltage of the "sensing channel" can be linearly tuned in a voltage window exceeding 0.4 V. We have demonstrated that the dual-gate structure enables a much better sensor response to the detachment of human mesenchymal stem cells. In general, the capability of tuning the optimal sensing bias will not only improve the device performance but also broaden the material selection for cell-based organic bioelectronics.

KEYWORDS: *electrolyte-gated organic field effect transistor, organic electrochemical transistor, dual-gate, cell sensing, threshold voltage tuning*

1. INTRODUCTION

Interfacing living cells and tissues with organic bioelectronics allows in situ sensing and recording of cell bioelectrical activities and opens opportunities for understanding biological processes in living cells, developing implantable prosthetic devices, and performing low-cost and efficient in vitro drug cytotoxicity tests.[1−4] Among various bioelectronic device structures, liquid electrolyte-gated organic field effect transistors (EGOFETs) and organic electrochemical transistors (OECTs) are particularly attractive for extracellular recording and stimulation because of their advantages in low voltage operation, self-signal amplification, biological compatibility, as well as mechanical and chemical flexibility. EGOFETs possess high sensitivity to the electrostatic potential variation at the interface of the organic semiconductor and the liquid electrolyte, where most sensing events take place.[5−7] In this device structure, the electrical double layer formed at the solid–liquid interface enables fast device response and low voltage operation.[8,9] OECTs, on the other hand, deliver large transconductance ($g_m = dI_D/dV_G$) through electrochemical doping induced by ion diffusion into the bulk semiconductor.[10−12] For both the OFET- and OECT-based cell-sensors, two operation modes could be used: ac and dc mode monitoring. The transient responses of OECTs to an ac gate pulse were used to assess the integrity of the barrier tissue[13] and diagnose epithelial infection.[14] Impedance spectroscopy with

Received: June 29, 2017
Accepted: October 17, 2017
Published: October 17, 2017

DOI: 10.1021/acsami.7b09384
ACS Appl. Mater. Interfaces 2017, 9, 38687−38694

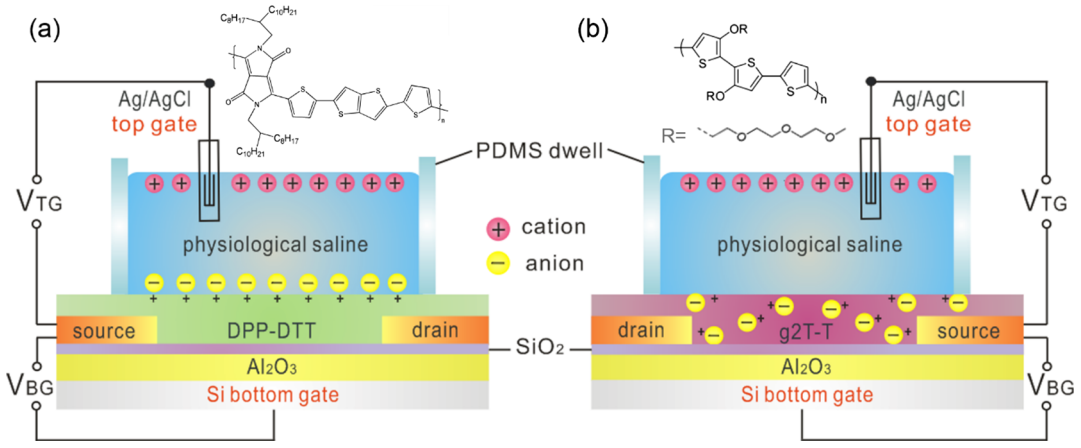

Figure 1. (a) Schematic cross section of a DG-OFET device and the chemical structure of DPP-DTT; (b) schematic cross section of a DG-OECT device and the chemical structure of g2T-T.

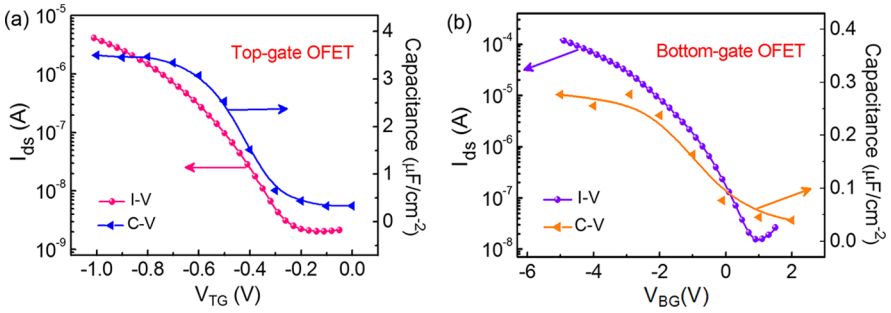

Figure 2. Transfer characteristics and effective capacitance−voltage ($C-V$) relations of (a) top-gate OFET and (b) bottom-gate OFET in the single-gate mode. The $C-V$ characteristics were measured at 1 Hz.

OFETs and OECTs has been utilized to monitor cellular activities, such as adhesion and coverage,[15,16] drug-induced apoptosis or monolayer disruption[17−19] and detachment.[20] On the other hand, a dc gate-bias was also used to turn the transistors on for applications such as mapping of neural circuits in real time,[21] monitoring of cardiac action potential,[22,23] and recording of transepithelial ion transport.[24] A crucial requirement for EGOFETs and OECTs in biosensing applications is that the applied voltage across the tissue or cell layer for prolonged time should be kept below 0.3 V (absolute value) to avoid undesired electrochemical processes that may cause membrane rupture and cell death.[25−27] (In our study, we also observed that a sensing gate voltage around 0.35 V damages the cells within 5 min whereas 0.3 V keeps the cells alive, as shown in Figure S1.) This cell fatality issue imposes a limit on the selection of organic semiconductors, allowing only those that exhibit desired threshold voltage to be used. As a result, most EGOFET-based cell sensors rely on pentacene, while a large variety of high mobility, biocompatible, and water-stable organic materials are not utilized. Similarly, the gate voltage corresponding to the maximum transconductance exceeds 0.3 V in some of the OECTs,[11,28] leaving the highest amplification point unavailable. (Note that although ac mode monitoring could, to a large extent, reduce the voltage damage to cells, it may still need a dc bias to reach the maximum amplification.)

In this work, we addressed the limitation on operation voltage by designing a solid−liquid dual-gate organic transistor structure. In this device structure, the threshold voltage of the liquid-gated conduction channel is controlled by an additional gate that is separated from the channel by a metal-oxide gate dielectric. We have demonstrated that with this design the threshold voltage can be linearly tuned in a voltage window exceeding 0.4 V, and the dual-gate structure enables a much better sensor response to detachment of human mesenchymal stem cells (hMSCs) as compared to the single-gate structure. The dual-gate design can also be extended to accumulation-mode OECT structures, enabling tuning of the maximum transconductance point to below 0.3 V.

2. RESULTS AND DISCUSSION

2.1. Fabrication of Dual-Gate Organic Field-Effect Transistors (DG-OFETs). Figure 1 shows the device structures developed in this study. For the DG-OFET, we used a high crystallinity copolymer, poly(*N*-alkyl diketopyrrolo-pyrrole-dithienylthieno[3,2-*b*]thiophene) (DPP-DTT),[29] as the semiconducting material; whereas for the dual-gate OECT (DG-OECT) device, we applied the semiconducting polymer poly(2,5-bis(3-triethyleneglycoloxythiophen-2-yl)-*co*-thiophene) g2T-T,[28] with hydrophilic side chains, as the active material. In the dual-gate design, an aluminum oxide (Al_2O_3, 50 nm)/silicon oxide (SiO_2, 10 nm) dielectric bilayer was employed to support the bottom-gate operation. The Al_2O_3 layer, formed through atomic layer deposition (ALD), was chosen because of its high dielectric constant of 8.9, allowing low voltage operation. A thin layer of SiO_2 was sputtered on top of the Al_2O_3 layer to facilitate the growth of an octyltrichlorosilane (OTS-8) self-assembled monolayer on the oxide surface, a modification process that is commonly used to reduce surface traps and improve the interface morphology for

DOI: 10.1021/acsami.7b09384
ACS Appl. Mater. Interfaces 2017, 9, 38687−38694

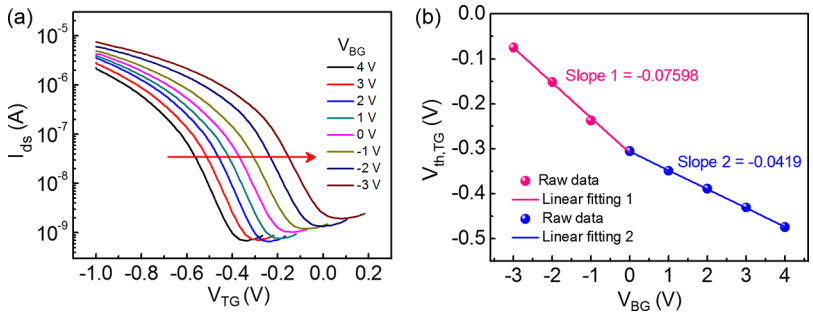

Figure 3. (a) Transfer characteristics of the top-gate OFET operated in the dual-gate mode with the bottom-gate bias varying from +4 to −3 V in steps of −1 V from left to right. The drain voltage was kept constant at −0.4 V; (b) linear dependence of the top-gate OFET threshold voltage on the bottom-gate bias (dots: data; lines: linear fitting).

OFETs.[30,31] For the top gate, a physiological saline solution [confined in a polydimethylsiloxane (PDMS) dwell] was used as the electrolyte and a Ag/AgCl reference electrode, immersed in the solution, was used as the gate electrode. To induce coupling between the top and bottom gate fields while maintaining efficient charge transport, the thickness of the semiconductor layer should be carefully tuned. We found that the optimal semiconductor thicknesses for the DG-OFET and DG-OECT structures are around 25 and 45 nm, respectively, which yield high field-effect mobility while at the same time allowing strong dual-gate effect.

2.2. Characterizations and Theoretical Analysis of DG-OFET. To understand the effects of individual gates, we first operated the DG-OFET device in the "top-gate only" and "bottom-gate only" modes. Figure 2 shows the current−voltage (I−V) and effective capacitance−voltage (C−V) characteristics of the devices. (The effective capacitance values were extracted based on a parallel resistor−capacitor model.) Note that in the single-gate test mode, the connection of the other gate (floated or grounded) has a little effect on the electrical characteristics of the devices, as shown in Figure S2. The effective areal capacitance densities of the bottom-gate dielectric and top-gate dielectric are measured to be 0.25 and 3.44 μF cm^{-2}, respectively, suggesting a stronger field effect of the top-gate OFET. The effective capacitance−frequency (C−F) characteristics of the devices and the corresponding impedance modulus and phase angles are shown in Figure S3. On the basis of the capacitance values, the extracted bottom and top FET mobilities are 0.149 and 0.021 cm^2 V^{-1} s^{-1}, respectively. There may be two reasons for such mobility differences. Firstly, the packing of the polymer chains at the bottom interface may be more ordered than that on the top interface; secondly, the saline solution may introduce trap states on the top interface, while the bottom interface is well-passivated by the OTS layer. We note from previous studies[32,33] that to achieve effective dual-gate operation, the top and bottom OFET channels should have comparable conductance, with the mobility difference less than 2 orders. Our DG-OFET device fulfills this requirement.

We now examine the device behavior in the dual-gate mode. As shown in Figure 3a, the threshold voltage ($V_{th,TG}$) of the top-gate OFET can be gradually tuned toward positive when the bottom-gate bias (V_{BG}) is varied from +4 to −3 V. Under a cell-friendly top-gate voltage of −0.2 V, the double-gated (V_{BG} = −3 V) channel current approaches ~10^{-7} A and the transconductance reaches 1.5 μS, 3 orders higher than that of the single-gated (V_{BG} floated). This tunability enables operation of the top-gate device at its most sensitive regime without damaging the biological species at the solid−liquid interface. The relationship between $V_{th,TG}$ and V_{BG} can be described with two linear fits, as presented in Figure 3b. The origin of the two linear relationships can be well-explained by analyzing the working principles of the dual-gate devices.[32,34,35] In a DG-OFET, both the top gate and bottom gate can induce a charge accumulation layer at their nearest semiconductor surface. If a negative bottom-gate voltage V_{BG} is applied and exceeds the threshold voltage (in our devices, the bottom-gate threshold voltage $V_{th,BG}$ is −0.25 V), a bottom accumulation channel is formed. Accordingly, to turn the entire device to the off state, a more positive top-gate bias (V_{TG}) is required, leading to a positive shift of $V_{th,TG}$. Such a relation can be described with the following equation[34]

$$\Delta V_{th,TG} = -\frac{C_{BG}}{C_{TG}}\Delta V_{BG} \quad (1)$$

where C_{BG} and C_{TG} represent the capacitances of the top and bottom channel, respectively. According to the capacitance values extracted from the C−V measurements, the ratio of C_{BG} to C_{TG} is 0.0727, agreeing well with the fitted slope of 0.07598 in Figure 3b.

As V_{BG} moves toward positive, the bottom-gate OFET is switched from accumulation to depletion, and the depletion electric field gradually penetrates into the semiconductor bulk. As a result, the top gate-accumulated charge carriers are depleted away by the bottom gate. The electrostatic coupling of the bottom-gate electric field and top-gate accumulation channel leads to a negative shift of $V_{th,TG}$ as described by the equations below[36,37]

$$\Delta V_{th,TG} = -\frac{C_{BG}C_{OSC}}{C_{TG}(C_{BG} + C_{OSC} + C_{BG\text{-}it})}\Delta V_{BG} \quad (2)$$

$$\frac{1}{C_{OSC}} = \frac{1}{C_{TG,depletion}} - \frac{1}{C_{TG,accumulation}} \quad (3)$$

$$C_{BG\text{-}it} = D_{BG\text{-}it} \times Q \quad (4)$$

where C_{TG} and C_{BG} are the capacitances of the top and bottom channel, respectively; $D_{BG\text{-}it}$ is the density of bottom interface states, $C_{BG\text{-}it}$ is the corresponding interface capacitance, and C_{OSC} is the depletion capacitance of the semiconductor. Here, C_{TG}, C_{BG}, and C_{OSC} can be extracted from the C−V characteristics given in Figure 2. On the basis of the fitted slope in the positive V_{BG} regime (blue line in Figure 3b), we calculate $D_{BG\text{-}it}$ to be 1.4 × 10^{11} cm^{-2} V^{-1}, similar to those reported for other organic devices.[38,39]

DOI: 10.1021/acsami.7b09384
ACS Appl. Mater. Interfaces 2017, 9, 38687−38694

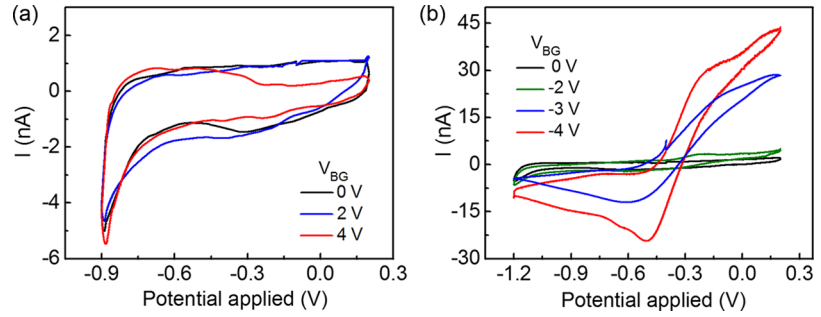

Figure 4. Cyclic voltammograms of the top-gate OFET at (a) positive bottom-gate biases and (b) negative bottom-gate biases.

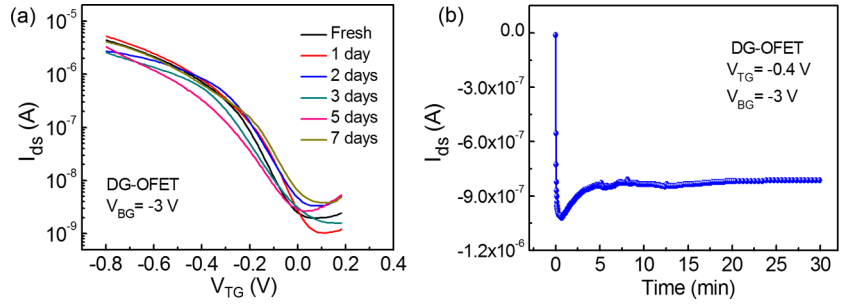

Figure 5. (a) Transfer characteristics of the DPP-DTT DG-OFET with V_{BG} = −3 V soaking in saline solution for 7 days. (b) Bias stress of the DPP-DTT DG-OFET for 30 min with V_{TG} = −0.4 V and V_{BG} = −3 V.

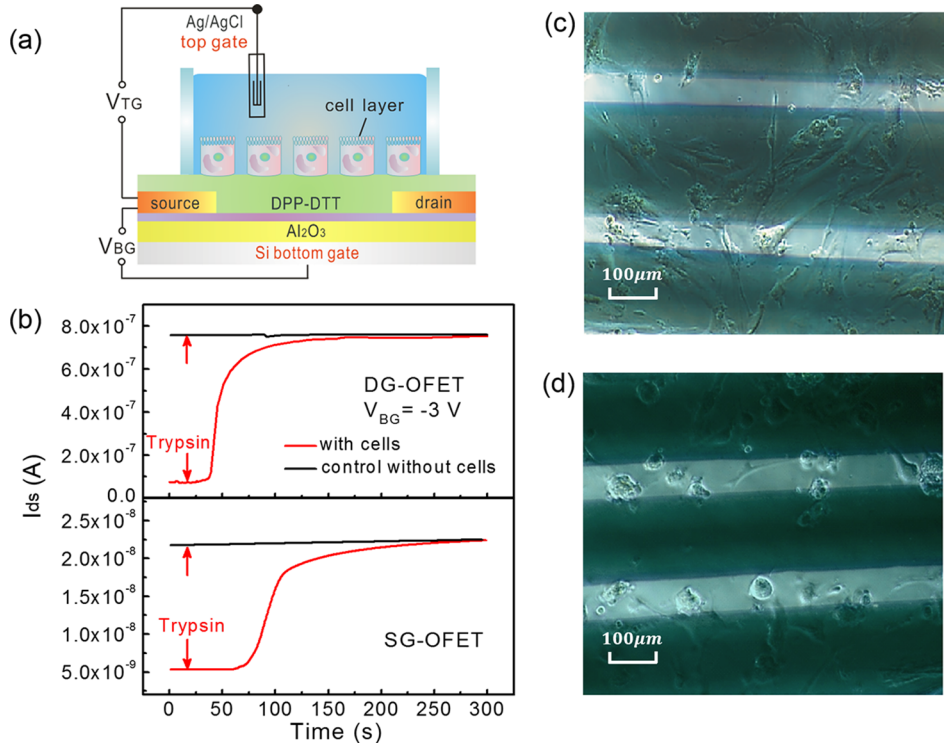

Figure 6. (a) Schematic diagram of the cell-sensing platform; (b) in situ responses of the DG-OFET (top) and SG-OFET (bottom) with (red trace) and without (black trace) hMSCs upon trypsin treatment (introduced at t = 20 s). For both devices, V_{ds} and V_{TG} were kept at −0.3 V; (c,d) optical images of hMSCs cultured on the FETs before and after 5 min of trypsin treatment, respectively.

2.3. Tuning Limit of the Top-Gate Threshold Voltage.

We found that increasing V_{BG} to above +3 V can further negatively shift $V_{th,TG}$, but decreasing V_{BG} to below −3 V will permanently destroy the device. To investigate the origin of this breakdown phenomenon, we performed cyclic voltammetry on the device at different V_{BG}. Figure 4a shows the cyclic voltammograms of the device under positive V_{BG}. It can be seen that no redox peak appears at positive bottom-gate biases, suggesting that the active layer is electrochemically stable within the voltage window and that the device is dominated by the OFET operation mechanism (i.e., the bulk polymer film is not electrochemically doped), as illustrated in Figure 1a. By

DOI: 10.1021/acsami.7b09384
ACS Appl. Mater. Interfaces 2017, 9, 38687−38694

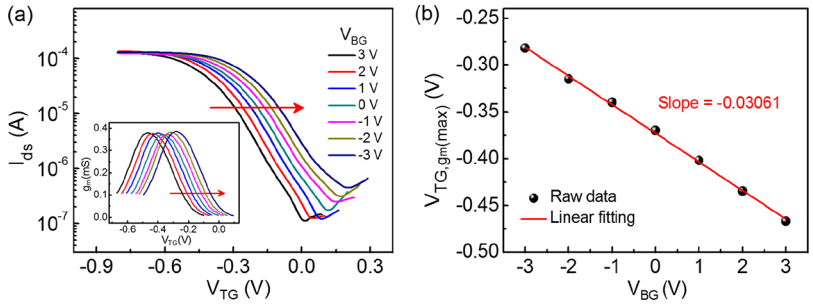

Figure 7. (a) Transfer curves of the top-gate OECT operated in the dual-gate mode with the bottom-gate bias varying from +3 to −3 V in steps of −1 V from left to right. The drain voltage is kept constant at −0.2 V. The inset figure shows the calculated transconductance corresponding to each transfer curve; (b) linear dependence of the maximum transconductance voltage point on the bottom-gate voltage. (Dots: data; line: linear fitting).

contrast, when V_{BG} is reduced to −3 V or below, redox peaks start to appear (Figure 4b). These peaks clearly indicate occurrence of electrochemical reactions, which, according to previous studies, involve holes in the semiconductor, water, oxygen, and protons.[40−42] Importantly, the protons produced at the surface of the oxide dielectric can penetrate into the oxide.[42,43] When the proton flux is large enough, the dielectric will breakdown. In fact, in our measurements, all the bottom-gate OFETs show very high leakage current after being operated in a double-gate mode with a negative V_{BG} below −3 V, confirming the breakdown of the oxide dielectric. The same phenomenon has also been observed in the DG-OFET devices employing thermal oxide (SiO_2) as the bottom-gate dielectric (see Figure S4). On the basis of such a redox reaction-induced voltage limit, one may speculate that it is advantageous to use a high-κ material as the bottom-gate dielectric, as it could induce a stronger bottom-gate effect on the DG-OFET device below the redox voltage threshold.

2.4. Stability Tests. Despite the high-voltage breakdown, the DG-OFET exhibits good operation stability. Figures 5a and S5 show the transfer characteristics and transconductance variation of the DG-OFET measured in a 7 day period, respectively. The device was immersed in a saline solution environment during the entire measurement period, and it exhibited similar transfer curves with the on−off ratio always above 10^3 and threshold voltage change of less than 0.08 V. The stable operation of the DG-OFET was also confirmed by monitoring the channel current consecutively for 30 min at V_{BG} = −3 V and V_{TG} = −0.4 V (Figure 5b). After the initial 4 min of bias stress, the current stabilized and remained almost unchanged for the rest of the stress period. Our device can also respond swiftly to the "on−off" gate voltage switching (Figure S6). We believe that the good stability of the device is associated with the compact and uniform morphology of the DPP-DTT film as well as its high molecular ordering, as revealed by the atomic force microscopy (AFM) and grazing incidence wide-angle X-ray scattering (GIWAXS) measurements (Figure S7). The measurements also reveal that the morphology and microstructure of the film remain similar before and after bias stress in saline solution. In addition, the performances of the DG-OFETs are highly reproducible. We measured the threshold voltage and mobility of the devices fabricated from 5 different batches (Figure S8 and Table S1) and found little variations in the results. All these observations confirm that the DPP-DTT DG-OFET provides a reliable platform in a biological environment, ensuring stable and reproducible sensing results.

2.5. Cell Detachment Sensing. To compare the cell-sensing performance of the dual-gate and single-gate device structures, we first cultivated hMSCs on top of the active layer, as shown in Figure 6a. The devices were characterized when 70% of the polymer surface was covered with hMSCs (Figure 6c). After cell seeding, the transfer characteristics of both devices were well-preserved, except that the gate field-effect was weakened (Figure S9a,c) because of the coverage of cells reducing the local ion concentration at the polymer−electrolyte interface. For the sensing experiment, 50 μL of trypsin solution was introduced into the saline reservoir to trigger cell detachment from the substrate (Figure 6d). To test the sensor response to the cell detachment, we recorded the variation of the FET current as a function of time. It can be seen from Figure 6b that the current of the DG-OFET is increased by 9 times from t = 38 s, whereas the corresponding current raise in the single-gate OFET (SG-OFET) is 3 times and occurs at t = 60 s. It is worth noting that, in general, the threshold voltage of the transistors is slightly increased (in absolute value) after cell growth (Figure S9). For the SG-OFET device, the threshold voltage is shifted to below −0.3 V; accordingly, the cell sensing is performed in the subthreshold regime, making the channel resistance of the FET insensitive to the small variations of the dielectric environment at the cell−polymer interface. As shown in Figure S9, only when the cells are completely detached from the polymer surface, the device current can be recovered to an on state. For the DG-OFET, on the other hand, the threshold voltage of the top-gate channel can be controlled to be close to zero via the bottom-gate bias. In this case, the resistance of the top-gate channel remains sensitive to the variation of the cell−polymer interface. Therefore, the device provides quick response when the connection between the cells and the polymer substrate is damaged. Finally, control experiments without cells (black data traces in Figure 6b) confirmed that the increase of the FET current was indeed caused by cell detachment.

2.6. Characterizations and Analysis of the DG-OECT. Finally, we examine whether the dual-gate effect can also be utilized to control the operation of OECTs. Here, we investigate the g2T-T-based DG-OECT structure shown in Figure 1b. This polymer has been previously shown to support p-type accumulation-mode OECT operation.[22] Figure 7a illustrates the top-gate transfer curves of the OECT under different bottom-gate voltages, and the inset shows the plot of the corresponding transconductance g_m. The result demonstrates again that with the additional gate, we are able to utilize the maximum device transconductance point within the cell-friendly voltage range. To quantitatively analyze the tuning of

DOI: 10.1021/acsami.7b09384
ACS Appl. Mater. Interfaces 2017, 9, 38687−38694

the maximum transconductance voltage point ($V_{TG,g_m(max)}$) by V_{BG}, we fit their relationship in Figure 7b. We note that, in this case, only one linear fit is required for all data points, which is different from the DG-OFET (Figure 3b). This is because in OECTs, ion-doping and dedoping occur in the entire active layer. As a result, the bottom-gate and top-gate effects are always coupled. A similar behavior has been reported previously in dual-gate self-assembled monolayer FETs (SAMFETs).[34,44] The relationship of $V_{TG,g_m(max)}$ and V_{BG} can thus be described by

$$\Delta V_{TG,g_m(max)} = -\frac{C_{BG}}{C_{TG}}\Delta V_{BG} \quad (5)$$

The effective areal capacitance densities of the bottom-gate and top-gate dielectrics are measured to be 0.35 and 11.2 μF cm^{-2} (Figure S10), respectively. The fitted slope of −0.03061 in Figure 7b agrees well with the ratio of C_{BG} to C_{TG} (0.03125), confirming the accuracy of the device model. We also performed the hMSC detachment sensing experiment using the g2T-T-based OECT devices (Figure S11) and found that the DG-OECT exhibits a larger current variation than the SG-OECT after cell detachment, which suggests that the dual-gate structure could improve the sensitivity of the OECT. However, the temporal response of the OECT sensing platforms is in general slower than that of the OFET platforms (shown in Figure 6), as the former involves a bulk-ion diffusion process.

3. CONCLUSIONS

In summary, we have demonstrated a liquid−solid dual-gate organic transistor structure to enable cell sensing with maximum transconductance (i.e. maximum amplification). In our device design, the threshold voltage of the top liquid-gated conduction channel is controlled by a bottom gate that is separated from the semiconductor with an Al_2O_3/SiO_2 bilayer gate dielectric. With this design, the threshold voltage of the "sensing channel" can be linearly tuned in a voltage window exceeding 0.4 V (from −0.475 to −0.074 V). It is found that the voltage tuning at the negative bottom-gate bias is limited by redox reactions that could permanently break the oxide gate dielectric. Within the breakdown threshold, in general, the operation of the DG-OFET and DG-OECT devices can be well-described with the device models developed for solid-state dual-gate transistors. We have demonstrated that the dual-gate structure enables a much better sensor response to the detachment of hMSCs. By applying the dual-gate concept to an aqueous sensing platform, we relax the original voltage limitation on the "liquid-gated" devices. This not only allows the use of a broader range of organic semiconductors with different surface potentials but also enables tuning the most sensitive detection point of a device to a cellular safe voltage.

4. EXPERIMENTAL METHODS

4.1. Device Fabrication. The syntheses of g2T-T and DPP-DTT have been reported in refs 22 and 23, respectively. Both the DG-OFET and DG-OECT exploit a heavily n-doped silicon wafer as the bottom-gate electrode, on top of which a 50 nm thick Al_2O_3 layer was grown using ALD at a growth temperature of 200°C. A thin layer (~10 nm) of SiO_2 was then sputtered on top of Al_2O_3 with an Anatech Magnetron Sputtering Machine in radio frequency mode under 100°C for 10 min to form the bilayer bottom-gate dielectric. Gold source and drain electrodes with a thickness of 30 nm were patterned by photolithography, yielding an interdigital structure of W/L = 10 × 1000 μm/40 μm. The oxide dielectric layers were passivated by immersing in 5 mM solution of OTS-8 in toluene for 24 h. After being sonicated in toluene and dried with nitrogen gas, the substrates with gold electrodes were immersed in 10 mM 1-octanethiol solution in isopropyl alcohol for 2 min. The semiconducting layers of the OFET and OECT were formed by spin-coating the DPP-DTT solution in 1,2-dichlorobenzene and the g2T-T solution in chloroform, respectively. A physiological saline solution, used as the electrolyte, was confined above the active area by a cylindrical PDMS reservoir with a radius of 1 mm. Finally, the dual-gate devices were completed by immersing the Ag/AgCl reference electrode into the electrolyte, serving as the top gate.

4.2. Device Characterization. Current−voltage characteristics were measured using a Keithley 2612B dual-channel system sourcemeter. Capacitance−voltage characteristics and cyclic voltammetry are measured with an impedance analyzer, Biologic SP-200, in a two-electrode configuration. The source and drain electrodes were shorted and connected to the counter electrode. The working electrode was connected to the top gate. A Keithley 2400 sourcemeter was used to apply voltage to the bottom gate in $I-V$ and cyclic voltammetry measurements.

4.3. Cell Culture and Seeding on the Device. hMSCs (Lonza, Allendale, New Jersey, USA) were expanded in a growth medium (a-MEM supplemented with 16.7% fetal bovine serum, 1% penicillin/streptomycin, and 1% L-glutamine) (Thermo Fisher Scientific, Waltham, Massachusetts, USA) and passaged every 7 days. Passage 4 hMSCs was used for seeding and adhesion on chips. We first sterilized the devices with 75% isopropanol before washing twice with sterilized phosphate-buffered saline (PBS) (Thermo Fisher Scientific). Then, hMSCs were trypsinized for 5 min after washing the Petri dish twice with sterilized PBS (Thermo Fisher Scientific) and collected by centrifuging the neutralized cell suspension at 500g for 3 min. The seeding density was 10 000 cells/cm^2. We resuspended the required amount of cells with around 30 μL of growth media, according to the area of the active layer, and injected cell suspension into PDMS molds. After overnight incubation at 37 °C, the growth media were renewed to get rid of nonadherent cells.

4.4. Cell Detachment Sensing. The channel current was monitored using a Keithley 2612B dual-channel system sourcemeter during the cell detachment process. The bottom-gate voltage was applied by a Keithley 2400 sourcemeter. The 2612B and 2400 sourcemeters were common grounded. All measurements were conducted at 37 °C, which was maintained by employing a hotplate. For trypsin treatment, we washed the cell-sensing devices with PBS and applied 50 μL of trypsin−ethylenediaminetetraacetic acid (0.05%, Thermo Fisher Scientific, Waltham, Massachusetts, USA) into the PDMS molds. The device without cells was used as the control. Cell detachment was confirmed by checking under the microscope (Nikon TE200 inverted fluorescence microscope, Tokyo, Japan) after trypsin treatment.

■ ASSOCIATED CONTENT

Supporting Information

The Supporting Information is available free of charge on the ACS Publications website at DOI: 10.1021/acsami.7b09384.

Effect of gate voltage to cells, characterizations of the single top-gate mode, capacitance−frequency ($C-F$) relation and the corresponding modulus and phase angles of the EGOFET, cyclic voltammograms of DG-OFET with SiO_2 bottom-gate dielectric, the transconductance of the DPP-DTT EGOFET versus time, response of EGOFET to on−off gate voltage, AFM and GIWAXS results, device reproducibility tests, OFET transfer relations with hMSCs and after cell detachment, capacitance−voltage and capacitance−frequency relation of the g2T-T OECT, cell detachment sensing on OECT (PDF)

DOI: 10.1021/acsami.7b09384
ACS Appl. Mater. Interfaces 2017, 9, 38687−38694

AUTHOR INFORMATION

Corresponding Author

*E-mail: nzhao@ee.cuhk.edu.hk.

ORCID

Liming Bian: 0000-0003-4739-0918
Iain McCulloch: 0000-0002-6340-7217
Ni Zhao: 0000-0002-1536-8516

Notes

The authors declare no competing financial interest.

ACKNOWLEDGMENTS

We gratefully acknowledge funding from the Research Grant Council of Hong Kong (grant no. CUHK14218716).

ABBREVIATIONS

EGOFET, electrolyte-gated organic field effect transistor; DG-OFET, dual-gate organic field effect transistor; DG-OECT, organic electrochemical transistors (OECTs); ALD, atomic layer deposition; AFM, atomic force microscopy; GIWAXS, grazing incidence wide-angle X-ray scattering

REFERENCES

(1) Simon, D. T.; Gabrielsson, E. O.; Tybrandt, K.; Berggren, M. Organic Bioelectronics: Bridging the Signaling Gap between Biology and Technology. *Chem. Rev.* **2016**, *116*, 13009−13041.

(2) Jonsson, A.; Song, Z.; Nilsson, D.; Meyerson, B. A.; Simon, D. T.; Linderoth, B.; Berggren, M. Therapy using Implanted Organic Bioelectronics. *Sci. Adv.* **2015**, *1*, No. e1500039.

(3) Rivnay, J.; Owens, R. M.; Malliaras, G. G. The Rise of Organic Bioelectronics. *Chem. Mater.* **2014**, *26*, 679−685.

(4) Patra, S.; Roy, E.; Karfa, P.; Kumar, S.; Madhuri, R.; Sharma, P. K. Dual-responsive Polymer Coated Superparamagnetic Nanoparticle for Targeted Drug Delivery and Hyperthermia Treatment. *ACS Appl. Mater. Interfaces* **2015**, *7*, 9235−9246.

(5) Buth, F.; Donner, A.; Sachsenhauser, M.; Stutzmann, M.; Garrido, J. A. Biofunctional Electrolyte-Gated Organic Field-Effect Transistors. *Adv. Mater.* **2012**, *24*, 4511−4517.

(6) Casalini, S.; Leonardi, F.; Cramer, T.; Biscarini, F. Organic Field-effect Transistor for Label-free Dopamine Sensing. *Org. Electron.* **2013**, *14*, 156−163.

(7) Kim, S. H.; Hong, K.; Lee, K. H.; Frisbie, C. D. Performance and Stability of Aerosol-jet-printed Electrolyte-gated Transistors based on Poly(3-hexylthiophene). *ACS Appl. Mater. Interfaces* **2013**, *5*, 6580−6585.

(8) Di Lauro, M.; Casalini, S.; Berto, M.; Campana, A.; Cramer, T.; Murgia, M.; Geoghegan, M.; Bortolotti, C. A.; Biscarini, F. The Substrate is a pH-Controlled Second Gate of Electrolyte-Gated Organic Field-effect Transistor. *ACS Appl. Mater. Interfaces* **2016**, *8*, 31783−31790.

(9) Leonardi, F.; Casalini, S.; Zhang, Q.; Galindo, S.; Gutiérrez, D.; Mas-Torrent, M. Electrolyte-Gated Organic Field-effect Transistor Based on a Solution Sheared Organic Semiconductor Blend. *Adv. Mater.* **2016**, *28*, 10311−10316.

(10) Giridharagopal, R.; Flagg, L. Q.; Harrison, J. S.; Ziffer, M. E.; Onorato, J.; Luscombe, C. K.; Ginger, D. S. Electrochemical Strain Microscopy Probes Morphology-induced Variations in Ion Uptake and Performance in Organic Electrochemical Transistors. *Nat. Mater.* **2017**, *16*, 737−742.

(11) Inal, S.; Rivnay, J.; Leleux, P.; Ferro, M.; Ramuz, M.; Brendel, J. C.; Schmidt, M. M.; Thelakkat, M.; Malliaras, G. G. A High Transconductance Accumulation Mode Electrochemical Transistor. *Adv. Mater.* **2014**, *26*, 7450−7455.

(12) Hütter, P. C.; Fian, A.; Gatterer, K.; Stadlober, B. Efficiency of the Switching Process in Organic Electrochemical Transistors. *ACS Appl. Mater. Interfaces* **2016**, *8*, 14071−14076.

(13) Jimison, L. H.; Tria, S. A.; Khodagholy, D.; Gurfinkel, M.; Lanzarini, E.; Hama, A.; Malliaras, G. G.; Owens, R. M. Measurement of Barrier Tissue Integrity with an Organic Electrochemical Transistor. *Adv. Mater.* **2012**, *24*, 5919−5923.

(14) Tria, S. A.; Ramuz, M.; Huerta, M.; Leleux, P.; Rivnay, J.; Jimison, L. H.; Hama, A.; Malliaras, G. G.; Owens, R. M. Dynamic Monitoring of Salmonella Typhimurium Infection of Polarized Epithelia using Organic Transistors. *Adv. Healthcare Mater.* **2014**, *3*, 1053−1060.

(15) Ramuz, M.; Hama, A.; Rivnay, J.; Leleux, P.; Owens, R. M. Monitoring of cell layer coverage and differentiation with the organic electrochemical transistor. *J. Mater. Chem. B* **2015**, *3*, 5971−5977.

(16) Law, J. K. Y.; Susloparova, A.; Vu, X. T.; Zhou, X.; Hempel, F.; Qu, B.; Hoth, M.; Ingebrandt, S. Human T cells monitored by impedance spectrometry using field-effect transistor arrays: a novel tool for single-cell adhesion and migration studies. *Biosens. Bioelectron.* **2015**, *67*, 170−176.

(17) Susloparova, A.; Koppenhöfer, D.; Vu, X. T.; Weil, M.; Ingebrandt, S. Impedance spectroscopy with field-effect transistor arrays for the analysis of anti-cancer drug action on individual cells. *Biosens. Bioelectron.* **2013**, *40*, 50−56.

(18) Rivnay, J.; Leleux, P.; Hama, A.; Ramuz, M.; Huerta, M.; Malliaras, G. G.; Owens, R. M. Using white noise to gate organic transistors for dynamic monitoring of cultured cell layers. *Sci. Rep.* **2015**, *5*, 11613.

(19) Rivnay, J.; Ramuz, M.; Leleux, P.; Hama, A.; Huerta, M.; Owens, R. M. Organic electrochemical transistors for cell-based impedance sensing. *Appl. Phys. Lett.* **2015**, *106*, 043301.

(20) Susloparova, A.; Koppenhöfer, D.; Law, J. K. Y.; Vu, X. T.; Ingebrandt, S. Electrical cell-substrate impedance sensing with field-effect transistors is able to unravel cellular adhesion and detachment processes on a single cell level. *Lab Chip* **2015**, *15*, 668−679.

(21) Qing, Q.; Pal, S. K.; Tian, B.; Duan, X.; Timko, B. P.; Cohen-Karni, T.; Murthy, V. N.; Lieber, C. M. Nanowire Transistor Arrays for Mapping Neural Circuits in Acute Brain Slices. *Proc. Natl. Acad. Sci. U.S.A.* **2010**, *107*, 1882−1887.

(22) Cohen-Karni, T.; Qing, Q.; Li, Q.; Fang, Y.; Lieber, C. M. Graphene and Nanowire Transistors for Cellular Interfaces and Electrical Recording. *Nano Lett.* **2010**, *10*, 1098−1102.

(23) Yao, C.; Li, Q.; Guo, J.; Yan, F.; Hsing, I.-M. Rigid and flexible organic electrochemical transistor arrays for monitoring action potentials from electrogenic cells. *Adv. Healthcare Mater.* **2015**, *4*, 528−533.

(24) Yao, C.; Xie, C.; Lin, P.; Yan, F.; Huang, P.; Hsing, I.-M. Organic Electrochemical Transistor Array for Recording Trans-epithelial Ion Transport of Human Airway Epithelial Cells. *Adv. Mater.* **2013**, *25*, 6575−6580.

(25) Bernards, D. A.; Malliaras, G. G.; Toombes, G. E. S.; Gruner, S. M. Gating of an Organic Transistor through a Bilayer Lipid Membrane with Ion Channels. *Appl. Phys. Lett.* **2006**, *89*, 053505.

(26) Benz, R.; Zimmermann, U. Pulse-length Dependence of the Electrical Breakdown in Lipid Bilayer Membranes. *Biochim. Biophys. Acta, Biomembr.* **1980**, *597*, 637−642.

(27) Benz, R.; Beckers, F.; Zimmermann, U. Reversible Electrical Breakdown of Lipid Bilayer Membranes: a Charge-pulse Relaxation Study. *J. Membr. Biol.* **1979**, *48*, 181−204.

(28) Nielsen, C. B.; Giovannitti, A.; Sbircea, D.-T.; Bandiello, E.; Niazi, M. R.; Hanifi, D. A.; Sessolo, M.; Amassian, A.; Malliaras, G. G.; Rivnay, J.; McCulloch, I. Molecular Design of Semiconducting Polymers for High-Performance Organic Electrochemical Transistors. *J. Am. Chem. Soc.* **2016**, *138*, 10252−10259.

(29) Li, J.; Zhao, Y.; Tan, H. S.; Guo, Y.; Di, C.-A.; Yu, G.; Liu, Y.; Lin, M.; Lim, S. H.; Zhou, Y.; Su, H.; Ong, B. S. A Stable Solution-processed Polymer Semiconductor with Record High-Mobility for Printed Transistors. *Sci. Rep.* **2012**, *2*, 754.

(30) Ito, Y.; Virkar, A. A.; Mannsfeld, S.; Oh, J. H.; Toney, M.; Locklin, J.; Bao, Z. Crystalline Ultrasmooth Self-assembled Monolayers of Alkylsilanes for Organic Field-effect Transistors. *J. Am. Chem. Soc.* **2009**, *131*, 9396−9404.

DOI: 10.1021/acsami.7b09384
ACS Appl. Mater. Interfaces 2017, 9, 38687−38694

(31) Yu, S. H.; Cho, J.; Sim, K. M.; Ha, J. U.; Chung, D. S. Morphology-driven High-performance Polymer Transistor-based Ammonia Gas Sensor. *ACS Appl. Mater. Interfaces* **2016**, *8*, 6570−6576.
(32) Maddalena, F.; Spijkman, M.; Brondijk, J. J.; Fonteijn, P.; Brouwer, F.; Hummelen, J. C.; de Leeuw, D. M.; Blom, P. W. M.; de Boer, B. Device Characteristics of Polymer Dual-gate Field-effect Transistors. *Org. Electron.* **2008**, *9*, 839−846.
(33) Gelinck, G. H.; van Veenendaal, E.; Coehoorn, R. Dual-gate Organic Thin-film Transistors. *Appl. Phys. Lett.* **2005**, *87*, 073508.
(34) Spijkman, M.-J.; Myny, K.; Smits, E. C. P.; Heremans, P.; Blom, P. W. M.; de Leeuw, D. M. Dual-Gate Thin-Film Transistors, Integrated Circuits and Sensors. *Adv. Mater.* **2011**, *23*, 3231−3242.
(35) Spijkman, M.-J.; Brondijk, J. J.; Geuns, T. C. T.; Smits, E. C. P.; Cramer, T.; Zerbetto, F.; Stoliar, P.; Biscarini, F.; Blom, P. W. M.; de Leeuw, D. M. Dual-gate Organic Field-effect Transistors as Potentiometric Sensors in Aqueous Solution. *Adv. Funct. Mater.* **2010**, *20*, 898−905.
(36) Lim, H.-K.; Fossum, J. G. Threshold Voltage of Thin-film Silicon-on-insulator (SOI) MOSFET's. *IEEE Trans. Electron Devices* **1983**, *30*, 1244−1251.
(37) Zhao, N. Field-Effect Transistors Based on Microcrystalline Conjugated Polymers. Ph.D. Thesis, University of Cambridge, UK, 2008.
(38) Völkel, A. R.; Street, R. A.; Knipp, D. Carrier Transport and Density of State Distributions in Pentacene Transistors. *Phys. Rev. B: Condens. Matter Mater. Phys.* **2002**, *66*, 195336.
(39) Garcia-Belmonte, G.; Boix, P. P.; Bisquert, J.; Sessolo, M.; Bolink, H. J. Simultaneous Determination of Carrier Lifetime and Electron Density-of-states in P3HT:PCBM Organic Solar Cells under Illumination by Impedance Spectroscopy. *Sol. Energy Mater. Sol. Cells* **2010**, *94*, 366−375.
(40) Sharma, A.; Mathijssen, S. G. J.; Cramer, T.; Kemerink, M.; de Leeuw, D. M.; Bobbert, P. A. Anomalous Current Transients in Organic Field-effect Transistors. *Appl. Phys. Lett.* **2010**, *96*, 103306.
(41) de Leeuw, D. M.; Simenon, M. M. J.; Brown, A. R.; Einerhand, R. E. F. Stability of n-type Doped Conducting Polymers and Consequences for Polymeric Microelectronic Devices. *Synth. Met.* **1997**, *87*, 53−59.
(42) Sharma, A.; Mathijssen, S. G. J.; Smits, E. C. P.; Kemerink, M.; de Leeuw, D. M.; Bobbert, P. A. Proton Migration Mechanism for Operational Instabilities in Organic Field-effect Transistors. *Phys. Rev. B: Condens. Matter Mater. Phys.* **2010**, *82*, 075322.
(43) Bobbert, P. A.; Sharma, A.; Mathijssen, S. G. J.; Kemerink, M.; de Leeuw, D. M. Operational Stability of Organic Field-Effect Transistors. *Adv. Mater.* **2012**, *24*, 1146−1158.
(44) Spijkman, M.; Mathijssen, S. G. J.; Smits, E. C. P.; Kemerink, M.; Blom, P. W. M.; de Leeuw, D. M. Monolayer Dual Gate Transistors with a Single Charge Transport Layer. *Appl. Phys. Lett.* **2010**, *96*, 143304.

DOI: 10.1021/acsami.7b09384
ACS Appl. Mater. Interfaces 2017, 9, 38687−38694